DOI: 10.1002/((please add manuscript number))
Article type: Communication

Crystalline, two-dimensional polyarylimide cathode for ultrastable and ultrafast Li storage

Gang Wang,[†] *Naisa Chandrasekhar,*[†] *Bishnu P. Biswal, Daniel Becker, Silvia Paasch, Eike Brunner, Matthew Addicoat, Minghao Yu, Reinhard Berger, and Xinliang Feng**

Dr. G. Wang, Dr. N. Chandrasekhar, Dr. B. Biswal, D. Becker, Dr. M. Yu, Dr. R. Berger, Prof. X. Feng
Center for Advancing Electronics Dresden (cfaed) & Department of Chemistry and Food Chemistry, Technische Universität Dresden, 01062 Dresden, Germany.
E-mail: xinliang.feng@tu-dresden.de
Dr. S. Paasch, Prof. E. Brunner
Chair of Bioanalytical Chemistry, Technische Universität Dresden, 01062, Dresden, Germany.
Dr. M. Addicoat
School of Science and Technology, Nottingham Trent University, Clifton Lane, Nottingham NG11 8NS, UK.

[†]G. Wang and N. Chandrasekhar contributed equally to this work.

Keywords: polyarylimide, 2D polymer, covalent organic frameworks, cathode, Li-ion batteries

Abstract

Organic electrode materials are of long-standing interest for next-generation sustainable lithium-ion batteries (LIBs). As a promising cathode candidate, imide compounds have attracted extensive attention due to their low cost, high theoretical capacity, high working voltage and fast redox reaction. However, the redox active site utilization of imide electrodes remains challenging to fulfill their potential applications. Herein we demonstrate the synthesis of a highly stable, crystalline two-dimensional polyarylimide (2D-PAI) integrated with carbon nanotube (CNT) for the use as cathode material in LIBs. The synthesized polyarylimide hybrid (2D-PAI@CNT) features with abundant π-conjugated redox-active naphthalene diimide units, robust cyclic imide linkage, high surface areas and well-defined accessible pores, which render the efficient utilization of redox active sites (82.9%), excellent structural stability and fast ion diffusion. As a consequence, high rate capability and ultrastable cycle

stability (100% capacity retention after 8000 cycles) are achieved in 2D-PAI@CNT cathode, which far exceeds the state-of-the-art polyimide electrodes. Our work may inspire the development of novel organic electrodes for sustainable and durable rechargeable batteries.

Organic electrode materials with multiple redox-active centers are highly promising for the next-generation sustainable Li-ion batteries (LIBs). Their scalable green synthesis and high structural flexibility enable controllably tuning battery parameters such as capacity, redox potential, kinetics and cycling stability through tailor-made molecular engineering.[1] Various organic electrode materials including organosulfur,[2] organic free radicals,[3] conjugated carbonyls[1b, 4] and conducting polymers[5] have been explored for rechargeable batteries. Among them, imide compounds containing carbonyl groups (C=O) have attracted extensive attention owing to their high theoretical capacity (two-electron redox process per imide center), high working voltage (~2.5 V) and fast redox reaction.[6] Nonetheless, the main challenge associated with imide electrodes lies in deficient redox-active site (C=O) utilization, especially at high current rates and during long-term operations, thus hindering their potential applications.

The active site utilization is generally affected by dissolution, chemical stability and ion-transport capability of organic electrodes. Small-molecular imide compounds always suffer from fast capacity fading due to severe dissolution into aprotic electrolytes, leading to low utilization of carbonyl active centers. Polyimides (PIs) with high molecular weight can largely suppress the solubility problem and improve the cycling performance.[4c, 6-7] Recently, two-dimensional polyarylimide-based covalent organic frameworks (2D-PAI COFs) have been explored for high-performance energy storage because of their tailorable redox building blocks, long-range ordered skeleton and well-defined nanopores.[8] Even though considerable efforts have been devoted to 2D-PAIs design from aspects of imide centers[9] and linkages[6],

the electrochemical stability of 2D-PAIs and retention of active sites during long-term operation remain to be enhanced. For example, boronate ester (B-O)-linked 2D-PAI COFs displayed a 50% capacity loss within 50 cycles;[10] and the microporous 2D-PAI COFs derived from tetraamino-benzoquinone and pyromellitic dianhydride (PMDA) also showed continuous capacity fading during cycling.[4a]

Herein, we report the synthesis of a crystalline 2D-PAI via a polycondensation reaction between tris(4-aminophenyl)amine (TAPA) and 1,4,5,8-naphthalenetetracarboxylic dianhydride (NTCDA). Driven by a π-π stacking interaction, the crystalline 2D-PAI can be readily integrated with carbon nanotube (2D-PAI@CNT) for application in LIBs (Figure 1). The resultant 2D-PAI@CNT displays tube-type core-shell morphology, a well-defined porous structure, a high surface area (768 m^2/g) and remarkable thermal/chemical stability. The unique porous structure of 2D-PAI@CNT provides short Li^+ diffusion pathway into its abundant carbonyl groups. When employed as cathode in LIBs, 2D-PAI@CNT shows a high reversible capacity of 104.4 mAh/g at 0.1 A/g, corresponding to an active site utilization of 82.9%. Remarkably, no capacity fading is observed after 8000 cycles at 0.5 A/g, which suggests superb electrochemical stability of 2D-PAI@CNT. Even at a high current rate of 2.0 A/g (~3 min charge/discharge), a capacity of 95.0 mAh/g can be delivered, indicating excellent Li^+ diffusion kinetics in 2D-PAI@CNT. To our knowledge, the cycling stability and rate capability of our 2D-PAI@CNT are among the best of all the PIs cathodes reported for rechargeable batteries.

The synthetic procedure towards 2D-PAI@CNT is illustrated in **Figure 1** and details are given in Supporting Information. In brief, a stable dispersion of CNT in a solvent mixture is pre-formed followed by addition of stoichiometric amounts of monomers TAPA and NTCDA. Then the dispersion was subjected to a heat treatment at 200 °C for 5 days. The pristine 2D-PAI is prepared under similar condition without using CNT. After careful optimization on solvent mixtures, it was found that a dimethylimidazolidone/mesitylene/iso-quinoline

(3:1:0.4) solvent system is optimal to achieve products with high crystallinity and superior surface areas (see Figure S1 and Table S1). The structural chemical integrity of 2D-PAI is identified by solid-state ^{13}C nuclear magnetic resonance spectroscopy (NMR, Figure S2). The peaks observed at 163.2 and 148.1 ppm derive from carbonyl carbon and C-N of 2D-PAI respectively. The overlapping peaks at 130.5 and 127.4 ppm are assigned to phenyl carbons of the incorporated building units (TAPA and NTCDA). Fourier transform infrared spectra (FTIR) of 2D-PAI and 2D-PAI@CNT both show three characteristic peaks at 1349, 1671 and 1717 cm^{-1} (Figure S3 and S4). The former peak originates from stretching vibration of the formed C–N–C moiety, while the latter two are from asymmetric/symmetric vibrations of C=O groups of the six-membered imide rings.

As shown in **Figure 2**a and Figure S5, the powder X-ray diffraction (XRD) patterns of 2D-PAI and 2D-PAI@CNT display good crystallinity with an intense peak at 2.98º, which corresponds to (110) reflection planes. The addition of CNT decreases the crystallinity of 2D-PAI@CNT and it was found that 50 wt% CNT is the threshold limit of crystallinity (Figure S5). Based on the obtained XRD patterns, 2D-PAI models were built and optimized using Self-Consistent Charge Density Functional Tight-Binding simulation method.[11] The experimental XRD patterns fit fairly well with the simulated structures derived from eclipsed AA stacking model (Figure 2a). The pore aperture (center-to-center distance) is ~2.54 nm and the interlayer π-π stacking distances vary from 3.8 to 4.0 Å (Figure S6). The lattice parameters of 2D-PAI are obtained to be a = 32.13 ± 0.1 Å, b = 32.32± 0.1 Å, c = 7.63 ± 0.03 Å; α = 89.77 ± 0.02º, β = 89.80 ± 0.02º, γ = 59.06 ± 0.01º using the Pawley refinement on Reflex module of BIOVIA Materials Studio 2017 (17.1.0.48. Copyright © 2016 Dassault Systèmes) (Figure 2a and Table S6-S8).

The porous structures of 2D-PAI and 2D-PAI@CNT were evaluated by nitrogen adsorption-desorption measurements at 77K (Figure 2b). 2D-PAI displayed a permanent porosity with reversible type-II isotherms and a Brunauer-Emmett-Teller (BET) surface area

of 1248 $m^2 g^{-1}$. The pore size distribution profile of 2D-PAI determined by non-local density functional theory (NLDFT) indicated pores of 1.25-2.85 nm (Figure 2c), which is close to the pore size of AA stacking model structure. The dominant pores centered at 1.7 nm account for the presence of slightly smaller and secondary pore void structures in 2D-PAI.[12] The BET surface area of 2D-PAI@CNT is determined as 768 $m^2 g^{-1}$, which is lower than 1248 $m^2 g^{-1}$ of pristine 2D-PAI due to the integration of CNT. 2D-PAI@CNT showed dominant pores at 1.7 and 2.7 nm along with the larger pores in the range of 4-12 nm, which derive from 2D-PAI and CNT, respectively. The pore size of 2.7 nm is very close to the predicted value for AA-stacked 2D-PAI. The thermogravimetric analysis (TGA) further reveals high thermal stability up to ~500 ^oC for both 2D-PAI and 2D-PAI@CNT (Figure S7). Besides, the 2D-PAI exhibits excellent chemical stability against various solvents, which is beneficial to electrode stability for battery application. No dissolution, structural decomposition or crystallinity deterioration was observed on 2D-PAI after exposure to water, aqueous acid and common organic solvents like N, N-dimethylformamide and N-methylpyrrolidone for 24 h (Figure 2d).

The morphology of 2D-PAI and 2D-PAI@CNT was characterized by scanning electron microscope (SEM). The pristine 2D-PAI consists of agglomeration of small nanoparticles (~50 nm), while 2D-PAI@CNT presents a tube structure (Figure S8). As further revealed by transmission electron microscope (TEM), small nano-crystallites of 2D-PAI (Figure 2e) and tube-type core-shell structures of 2D-PAI@CNT can be clearly visualized (Figure 2f). And a layer of 4-6 nm 2D-PAI was coated on the surface of CNTs. The formation of 2D-PAI@CNT can be accomplished in the following manner: the strong π-π interaction between 2D-PAI and CNTs drives the heterogeneous nucleation and growth of 2D-PAI on CNTs, which is more energetically favorable than the homogeneous nucleation/growth process in solution.[13] Moreover, energy dispersive X-Ray mapping analysis (carbon, nitrogen and oxygen) evidences the uniform distribution of 2D-PAI on CNTs (Figure S10).

The electrochemical performances of 2D-PAI and 2D-PAI@CNT were then evaluated in a potential window of 1.5-3.5 V in coin cells with Li foil as the counter electrode. The electrolyte is 1.0 M lithium bis(trifluoromethanesulfonyl)imide in 1,3-dioxolane and dimethoxyethane (v/v=1:1). Figure 3a shows the cyclic voltammetry (CV) curves of 2D-PAI and 2D-PAI@CNT at 1 mV/s. Compared to one redox couple of 2D-PAI, two broad redox bands consisting of two pairs of closely overlapped peaks are observed for 2D-PAI@CNT, which can be assigned to the reversible formation of radical anion (I^-) and dianion (I^{2-})[6]. Even though it is a two-step oxidation/reduction process of carbonyl groups, the fast transformation between I^- and I^{2-} results in wide overlap of redox peaks. Further, 2D-PAI@CNT represents smaller peak voltage gaps of redox couples and larger CV area than 2D-PAI, indicating lower polarization and more efficient utilization of redox active sites in 2D-PAI@CNT.

In the galvanostatic charge-discharge test, both 2D-PAI and 2D-PAI@CNT cathodes show a single charge/discharge plateau (Figure 3b), which agrees well with the CV result. The midpoint discharge voltage of 2D-PAI and 2D-PAI@CNT is ~2.4 V and similar to other reported PI cathodes (Table S2). At the current density of 0.1 A/g, the pristine 2D-PAI cathode delivers a limited capacity of 28.5 mAh/g, corresponding to low utilization of active sites (22.6%). This can be mainly attributed to the poor electrical conductivity of PIs.[14] Notably, a ~100% capacity retention is achieved on 2D-PAI after 50 cycles (Figure 3c), which indicates remarkable chemical stability of 2D-PAI. Such cycling stability of 2D-PAI is superior to the reported B-O linked COF[10] and fast capacity-fading monomers (TAPA and NTCDA, Figure S11). To improve the active site utilization of 2D-Pai, directly mixing 2D-Pai with CNTs (2D-PAI/CNT) in a mass ratio of 1:1 only slightly increased the capacity (65.6 mAh g^{-1}) and led to a high charge transfer resistance (Figure S12). hybridizing 2D-PAI with CNTs, the reversible capacity is largely enhanced to 104.4 mAh/g for 2D-PAI@CNT while maintaining the excellent cycling stability of 2D-PAI (Figure 3c). The active site utilization

degree of 2D-PAI@CNT is estimated to be ~82.9% with capacity contribution of CNT expelled (12 mAh/g, Figure S13). The long-term cycling performance of 2D-PAI@CNT is further evaluated at 0.5 A/g (Figure 3d). During the operation period over 4 months, high capacities over 100 mAh/g could be still achieved and no capacity fading was observed on 2D-PAI@CNT cathode during 8000 cycles, implying ultrastable active site utilization (>80%) in 2D-PAI@CNT. Our 2D-PAI@CNT exhibited the best cycling performance among all the reported PI electrodes for rechargeable batteries (Figure 3e and Table S2).

In addition, the cycling stability of 2D-PAI hybrid was found sensitive to the conjugated imide cores. As a control sample, PI-PMDA@CNT was synthesized from pyromellitic dianhydride (PMDA) instead of NTCDA (see SI for synthesis details, Scheme S2 and S4) and characterized (Figure S14, Table S1). The PI-PMDA@CNT shows two pairs of well-resolved redox peaks on CV curves and two charge/discharge plateaus noticed on galvanostatic charge-discharge curves (Figure S15a, b). In contrast to the stable cycling behavior of 2D-PAI@CNT, the PI-PMDA@CNT demonstrates an initial discharge capacity of 80.9 mAh/g and a capacity loss of 20% within 50 cycles (Figure S15c). The inferior cycling stability of PI-PMDA@CNT to NTCDA-derived 2D-PAI@CNT can be explained by the following: in the lithiation states, the five-membered lithium enolates from PI-PMDA show weaker resonance degree and less aromaticity than the six-membered conjugated lithium enolates from 2D-PAI, thus leading to higher intramolecular tension and inferior stability (Figure S16).[1b, 15] This is likely the reason why PMDA-derived PIs always suffers from an unsatisfied cycling stability (Table S3). Even compared with other NTCDA-derived PIs using different linkages (imine, boronate ester), our 2D-PAI shows better capacity retention (Table S4). The propeller-shaped triphenyl amine units with cyclic imide linkage may also help to alleviate tension within the whole 2D framework, thus promoting chemical stability of 2D-PAI.

To gain insight into the potential structural change of 2D-PAI@CNT cathodes after the long-term cycling test, we performed various characterizations on the cycled electrodes. The FTIR

spectra of 2D-PAI@CNT electrode before and after 8000 cycles (Figure S17) revealed that the characteristic stretching bands of carbonyl and C-N-C were retained. The XRD patterns of 2D-PAI@CNT also showed similar crystalline structure before and after cycling test (Figure S18). As confirmed by the SEM image (Figure S19), the tube-shape morphology of 2D-PAI@CNT was well maintained after continuous charge-discharge operation. All these results imply excellent structure stability of 2D-PAI@CNT.

The rate capability of 2D-PAI@CNT was then investigated under various current rates (Figure 3f and g). 2D-PAI@CNT shows capacitor-like high power features that the capacity is less dependent on the current. Increasing the current from 0.2 to 2 A/g, the reversible capacity slightly decreased from 104 to 95 mAh/g with a high active carbonyl utilization of >75%. In addition, the charge-discharge curves remained the similar shape without obvious polarization (Figure 3f), signifying the excellent transport properties of both Li ions and electrons within the 2D-PAI@CNT electrodes. The rate capability of 2D-PAI@CNT is also superior to those of the recently reported high-performance PI cathodes (Figure 3h and Table S5). In order to understand the fast rate capability, the electrochemical reaction kinetics of 2D-PAI@CNT was investigated by CV measurements. The current response (i) of 2D-PAI@CNT to the applied sweep rate (v, 0.1-1.0 mV/s) was analyzed (Figure 4a). According to the power law, $i = av^b$, a redox reaction limited by semi-infinite linear diffusion gives a b value of 0.5, while for a capacitive process, the b value is 1.[16] The b values of four redox peaks (0.97, 1, 0.98 and 0.96) are all close to 1 (Figure 4b). It means that the charge storage in 2D-PAI@CNT is a fast surface-controlled pseudocapacitive process, which results from unlimited ion diffusion in aligned-channels and high reactivity of imide centers in 2D-PAI@CNT. According to the equation $i = k_1v+k_2v^{1/2}$, the exact capacitive contribution (k_1v) can be further quantified, where k_1 and k_2 constants can be simulated by plotting $iv^{-1/2}$ vs $v^{1/2}$. At 0.1 mV/s, the capacitive contribution is determined to be 94.8%, which is further enhanced to 98.5% at 1

mV/s. These results suggest that Li storage in 2D-PAI@CNT is a kinetically fast pseudocapacitive process.

In summary, we have synthesized a novel crystalline 2D-PAI@CNT hybrid for application in Li-ion batteries. The 2D-PAI@CNT is featured with abundant redox-active naphthalene diimide carbonyl centers, high surface area and well-defined porous channels, which enable stable and high active site utilization during charge storage. Notably, both the stable imide cores and robust linkage contribute to the superior structural stability of 2D-PAI@CNT, making it the most stable and efficient PI cathode for LIBs. Further, the Li storage in 2D-PAI@CNT is revealed as a fast pseudocapacitive process. The key finding and active site stabilization strategy presented in this work can be readily extended to other organic electrode systems for developing high-performance rechargeable Na, K, Mg and Al-ion batteries.

Supporting Information
Supporting Information is available from the Wiley Online Library or from the author.

Acknowledgements
This work was financially supported by the ERC grant for HIPER-G (Project ID 768930), the innovation program under grant agreement No 696656 and 785219 (Graphene Flagship Core 1&2), the Federal State of Saxony (ESF-Project "GRAPHD", TU Dresden). We thank Mingchao Wang, Dr. Renhao Dong, and Dr. Lars Borchardt for helpful discussions. We thank Dr. Philipp Schlender, Dr. Markus Löffler and Dr. Petr Formanek, Dr. Sven Grätzfor XRD, SEM, TEM and BET measurements. The authors acknowledge the CFAED and the Dresden Center for Nanoanalysis (DCN) at TU Dresden.

Received: ((will be filled in by the editorial staff))
Revised: ((will be filled in by the editorial staff))
Published online: ((will be filled in by the editorial staff))

References

[1] a) Y. Liang, Z. Tao, J. Chen, *Adv. Energy Mater.* **2012**, *2*, 742-769; b) Q. Zhao, Z. Zhu, J. Chen, *Adv. Mater.* **2017**, *29*, 1607007; c) Q. Zhao, Y. Lu, J. Chen, *Adv. Energy Mater.* **2016**, 1601792; d) J. Kim, J. H. Kim, K. Ariga, *Joule* **2017**, *1*, 739-768. (e) H.-

G.Wang, S.Yuan, Z. Si, X.-B. Zhang, *Energy Environ. Sci.* **2015**, 8, 3160; (f) T. Sun, Z.-J.Li, H.-G. Wang, D. Bao, F.-L. Meng, X.-B. Zhang, Angew. Chem, Int. Ed. 2016, 128, 10820; (g) T. Sun, Z.-J. Li, X.-B. Zhang, *Research* **2018**, 2018, 10; (h) X.-L. Huang, D. Xu, S. Yuan, D.-L. Ma. S. wang, H.-Y.Zheng, X.-B. Zhang, *Adv. Mater.* **2014**, *26*, 7264.

[2] a) N. Oyama, J. M. Pope, T. Sotomura, *J. Electrochem. Soc.* **1997**, *144*, L47-L51; b) H. Kim, J. Lee, H. Ahn, O. Kim, M. J. Park, *Nat. Commun.* **2015**, *6*, 7278; c) R. H. Dong, M. Pfeffermann, D. Skidin, F. X. Wang, Y. B. Fu, A. Narita, M. Tommasini, F. Moresco, G. Cuniberti, R. Berger, K. Mullen, X. L. Feng, *J. Am. Chem. Soc.* **2017**, *139*, 2168-2171; d) M. B. Preefer, B. Oschmann, C. J. Hawker, R. Seshadri, F. Wudl, *Angew. Chem. Int. Ed. Engl.* **2017**, *56*, 15118-15122.

[3] a) J. Luo, B. Hu, C. Debruler, T. L. Liu, *Angew. Chem. Int. Ed. Engl.* **2018**, *57*, 231-235; b) M. Milton, Q. Cheng, Y. Yang, C. Nuckolls, R. Hernandez Sanchez, T. J. Sisto, *Nano Lett.* **2017**, *17*, 7859-7863.

[4] a) Z. Luo, L. Liu, J. Ning, K. Lei, Y. Lu, F. Li, J. Chen, *Angew. Chem. Int. Ed. Engl.* **2018**, *57*, 9443-9446; b) K. Amin, Q. Meng, A. Ahmad, M. Cheng, M. Zhang, L. Mao, K. Lu, Z. Wei, *Adv. Mater.*, 1703868; c) H.-g. Wang, S. Yuan, D.-l. Ma, X.-l. Huang, F.-l. Meng, X.-b. Zhang, *Adv. Energy Mater.* **2014**, *4*, 1301651.

[5] a) Z. Chen, J. W. F. To, C. Wang, Z. D. Lu, N. Liu, A. Chortos, L. J. Pan, F. Wei, Y. Cui, Z. N. Bao, *Adv. Energy Mater.* **2014**, *4*, 1400207; b) P. Novák, K. Müller, K. S. V. Santhanam, O. Haas, *Chem. Rev.* **1997**, *97*, 207-282; c) S. Liu, F. Wang, R. Dong, T. Zhang, J. Zhang, X. Zhuang, Y. Mai, X. Feng, *Adv. Mater.* **2016**, *28*, 8365-8370.

[6] Z. Song, H. Zhan, Y. Zhou, *Angew. Chem.* **2010**, *122*, 8622-8626.

[7] a) H. Wu, Q. Meng, Q. Yang, M. Zhang, K. Lu, Z. Wei, *Adv. Mater.* **2015**, *27*, 6504-6510; b) H. Wu, K. Wang, Y. Meng, K. Lu, Z. Wei, *J. Mater. Chem. A* **2013**, *1*, 6366-

6372; c) Z. Song, T. Xu, M. L. Gordin, Y.-B. Jiang, I.-T. Bae, Q. Xiao, H. Zhan, J. Liu, D. Wang, *Nano Lett.* **2012**, *12*, 2205-2211.

[8] S. Wang, Q. Wang, P. Shao, Y. Han, X. Gao, L. Ma, S. Yuan, X. Ma, J. Zhou, X. Feng, B. Wang, *J. Am. Chem. Soc.* **2017**, *139*, 4258-4261.

[9] X. Fan, F. Wang, X. Ji, R. Wang, T. Gao, S. Hou, J. Chen, T. Deng, X. Li, L. Chen, C. Luo, L. Wang, C. Wang, *Angew. Chem. Int. Ed. Engl.* **2018**, *57*, 7146-7150.

[10] F. Xu, S. Jin, H. Zhong, D. Wu, X. Yang, X. Chen, H. Wei, R. Fu, D. Jiang, *Sci. Rep.* **2015**, *5*, 8225.

[11] a) L. Sarkisov, A. Harrison, *Mol. Simulat.* **2011**, *37*, 1248-1257; b) B. Lukose, A. Kuc, T. Heine, *Chem. Eur. J.* **2011**, *17*, 2388-2392.

[12] L. Jiang, Y. Tian, T. Sun, Y. Zhu, H. Ren, X. Zou, Y. Ma, K. R. Meihaus, J. R. Long, G. Zhu, *J. Am. Chem. Soc.* **2018**, *140*, 15724-15730.

[13] a) G. Wang, J. Zhang, S. Yang, F. Wang, X. Zhuang, K. Müllen, X. Feng, *Adv. Energy Mater.* **2018**, *8*, 1702254; b) G. Wang, Y. Sun, D. Li, H.-W. Liang, R. Dong, X. Feng, K. Müllen, *Angew. Chem. Int. Ed.* **2015**, *54*, 15191-15196.

[14] C. Dongyang, A. Alyssa‐Jennifer, C. Zonghai, S. Junling, W. Shuanjin, X. Min, E. Zach, A. M. M., N. M. S., A. Khalil, M. Yuezhong, S. J. Fraser, *Adv. Mater.* **2015**, *27*, 2907-2912.

[15] S.-c. Chen, Q. Zhang, Q. Zheng, C. Tang, C.-Z. Lu, *Chem. Commun.* **2012**, *48*, 1254-1256.

[16] a) V. Augustyn, J. Come, M. A. Lowe, J. W. Kim, P.-L. Taberna, S. H. Tolbert, H. D. Abruña, P. Simon, B. Dunn, *Nat. Mater.* **2013**, *12*, 518-522; b) G. Wang, M. Yu, J. Wang, D. Li, D. Tan, M. Loffler, X. Zhuang, K. Mullen, X. Feng, *Adv. Mater.* **2018**, *30*, 1800533.

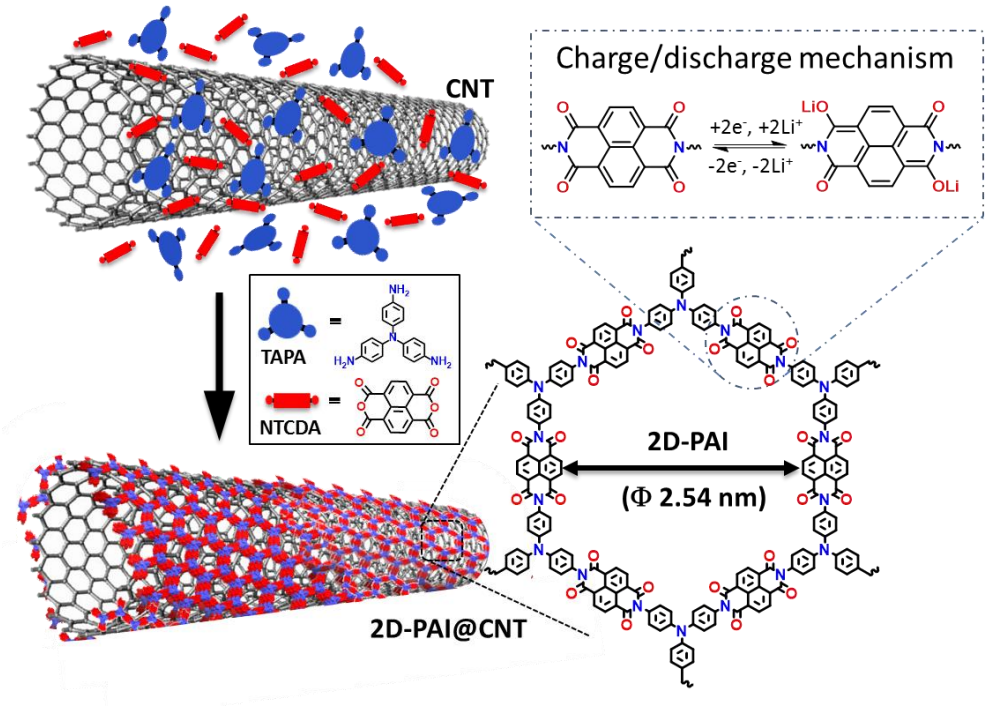

Figure 1. Schematic illustration of synthesis of crystalline 2D-PAI@CNT and energy storage process.

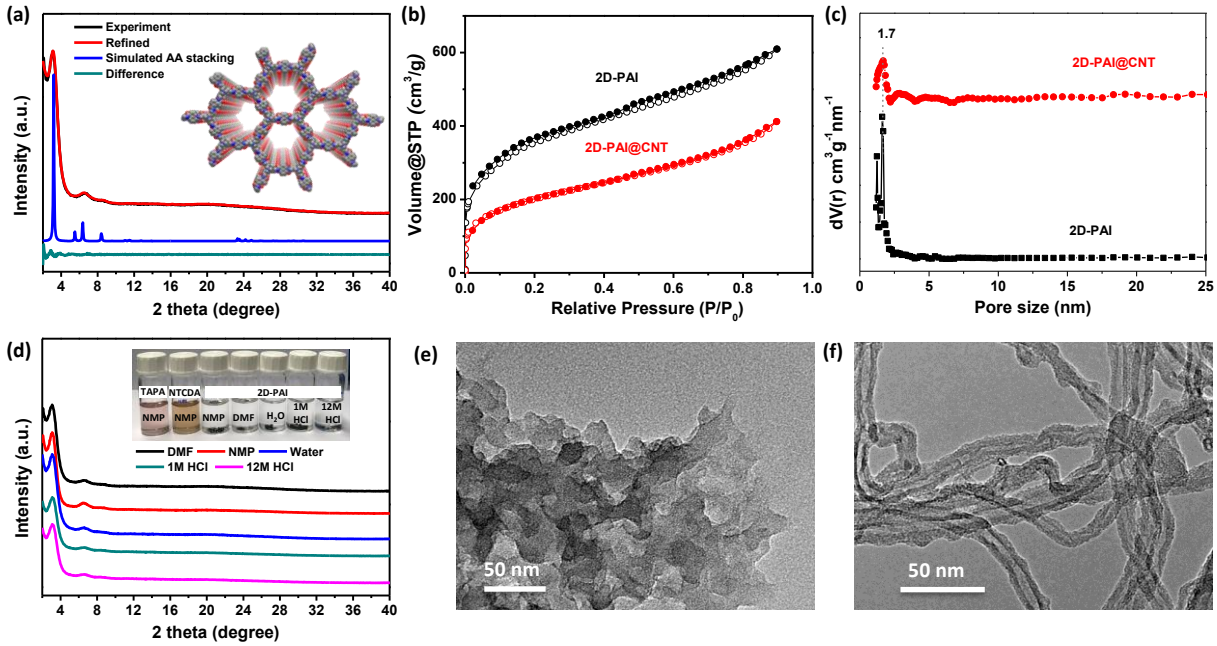

Figure 2. Structural features of 2D-PAI and 2D-PAI@CNT. (a) Experimental and simulated XRD patterns of 2D-PAI; Inset is illustration of the AA stacking model for 2D-PAI; (b) N_2 adsorption-desorption isotherms and (c) the pore-size distribution of 2D-PAI and 2D-PAI@CNT; (d) chemical stability of 2D-PAI; (e, f) TEM images of pristine 2D-PAI and 2D-PAI@CNT.

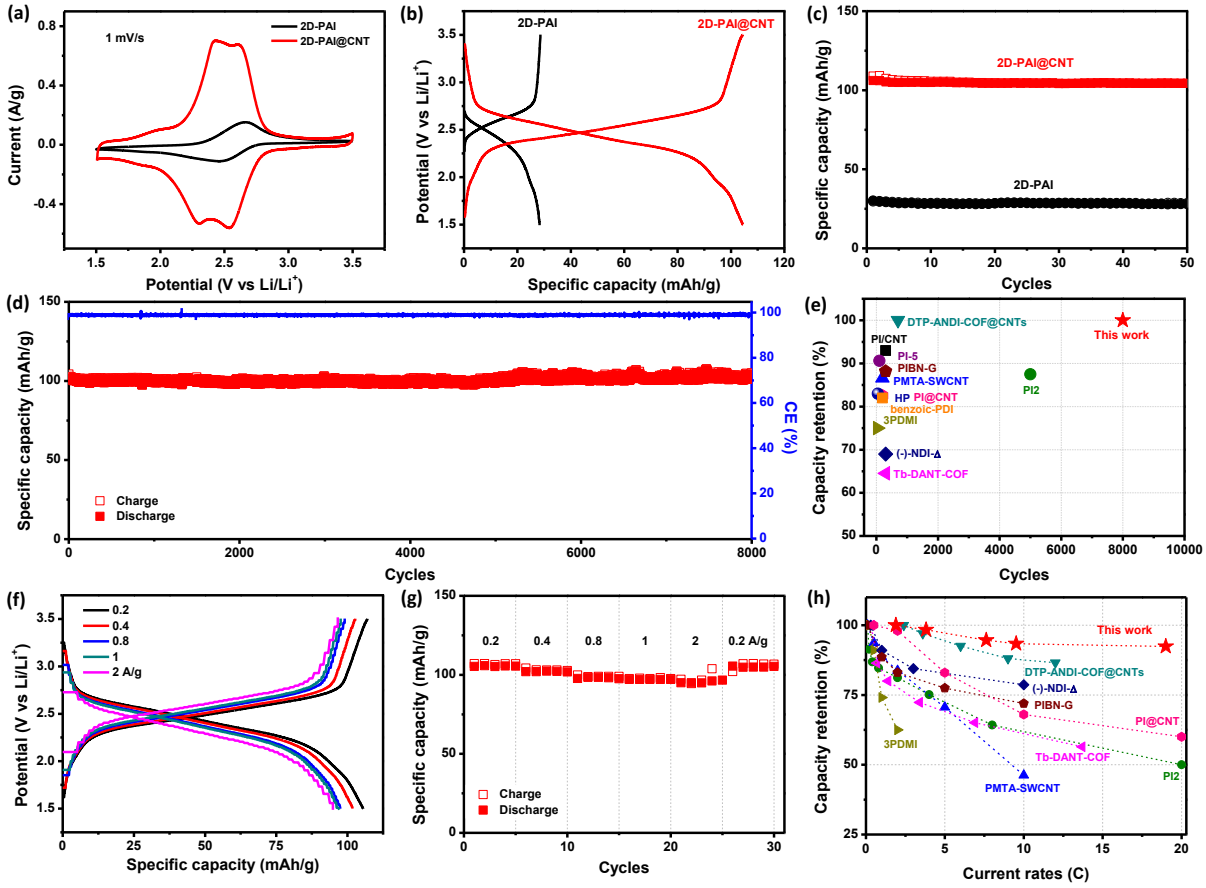

Figure 3. Electrochemical performance of 2D-PAI and 2D-PAI@CNT. (a) CV curves at 1 mV/s, (b) galvanostatic charge-discharge curves and (c) cycling performance of 2D-PAI and 2D-PAI@CNT at 0.1 A/g; (d) long-term cycling stability of 2D-PAI@CNT at 0.5 A/g; (e) cycling performance comparison with other PI cathodes; (f) charge-discharge curves at various current rates, (g) rate performance and (h) rate capability comparison of 2D-PAI@CNT with reported PI cathodes.

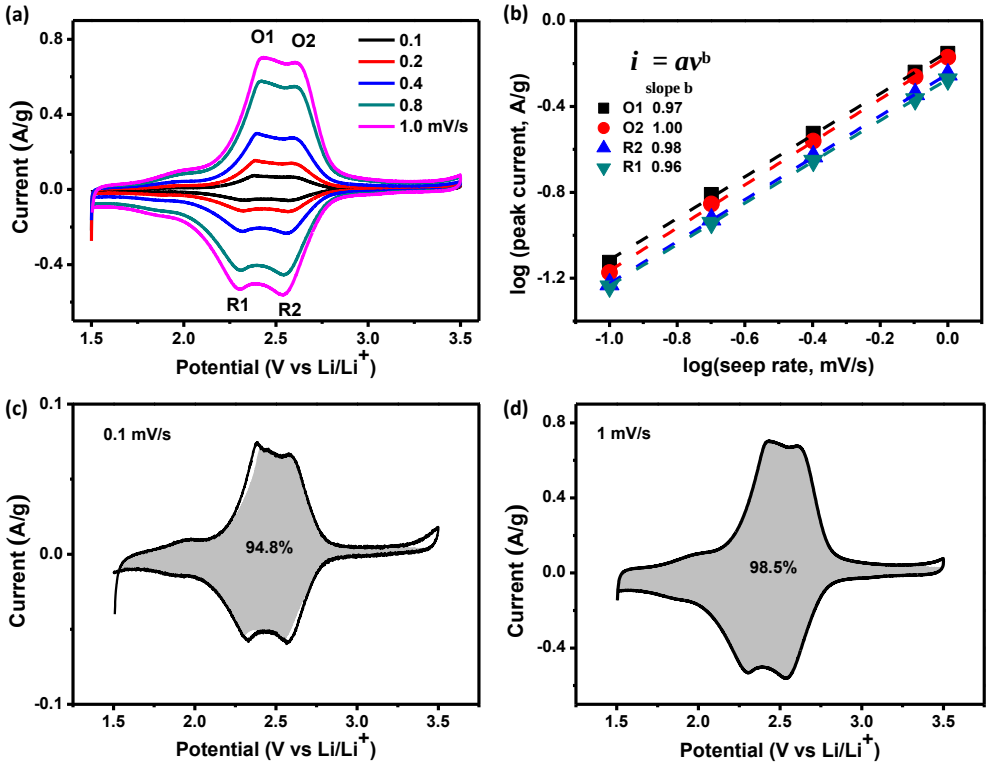

Figure 4. Kinetics and quantitative mechanism analysis. (a) CV curves of 2D-PAI@CNT collected under different scan rates; (b) log *i* versus log *v* plots to determine the b values of different peaks; (c, d) separation of capacitive and diffusion currents at 0.1 and 1 mV/s.

Crystalline two-dimensional polyarylimide integrated with carbon nanotube (2D-PAI@CNT) is prepared via in-situ synthesis and is explored as cathode for Li-ion batteries. The abundant redox active sites, robust framework made from imide cores/cyclic linkage, and well-defined porous structure endow 2D-PAI@CNT with ultrastable cycling stability and excellent rate capability to store Li charges, outperforming state-of-the-art polyimide cathodes for rechargeable batteries.

Polyarylimide cathode

Gang Wang, Naisa Chandrasekhar, Bishnu P. Biswal, Daniel Becker, Silvia Paasch, Eike Brunner, Matthew Addicoat, Minghao Yu, Reinhard Berger, Xinliang Feng*

Crystalline, two-dimensional polyarylimide cathode for ultrastable and ultrafast Li storage